Applied Radiation and Isotopes 210 (2024) 111377

Contents lists available at ScienceDirect

Applied Radiation and Isotopes

journal homepage: www.elsevier.com/locate/apradiso

Improving the detection limit in lung counting with a segmented HPGe detector

Henri Jutila [a,b,*], Paul Greenlees [a,b], Tiina Torvela [c], Maarit Muikku [c]

[a] Accelerator Laboratory, Department of Physics, University of Jyväskylä, FI-40014 Jyväskylä, Finland
[b] Helsinki Institute of Physics, University of Helsinki, P.O. Box 64, FI-00014 Helsinki, Finland
[c] STUK – Radiation and Nuclear Safety Authority, Jokiniemenkuja 1, FI-01370 Vantaa, Finland

ARTICLE INFO

Keywords:
Lung counting
Geant4 simulation
Voxel phantom
Segmented HPGe detector
MDA

ABSTRACT

A segmented High-Purity Germanium (HPGe) detector with a thin front segment together with various active and passive shield configurations was simulated with the aim of reducing the level of background events in lung counting applications. Eight different detector models were tested in a Geant4 simulation environment in a scenario where inhaled ^{241}Am activity was deposited in the lungs of an ICRP adult reference computational phantom. In lung counting measurements, the Compton continuum in the spectrum is generated by the natural and man-made radionuclides inside the human body and the natural background radiation from the environment. The reduction in Minimum Detectable Activity (MDA) using the segmented HPGe detector combined with an active shield compared to a model with a single germanium crystal was investigated. A reduction in MDA up to 30% and 66% was obtained for internal and external sources, respectively. The results show that the detection limit and/or the measurement time in lung counting can be reduced using such a detector configuration. Furthermore, combining the segmented HPGe detector with an active shield would be particularly useful in field measurements.

1. Introduction

In the case of nuclear accidents, people working in the nuclear industry and facilities that produce or handle radioactive material are most likely to be exposed to radioactivity with long biological half-lives via inhalation or ingestion. Therefore, a fast and reliable method is needed to determine the level and magnitude of the exposure. One approach is regular body counting, but radionuclides which emit low-energy gamma rays are difficult to measure. This issue can be overcome by lung counting (ICRU, 2003) which aims to determine the level of contamination in the human body directly via gamma radiation using High-Purity Germanium (HPGe) detectors. However, detecting radionuclides via low-energy gamma rays through the chest wall is difficult and if the intake occurred via ingestion, nothing is detected in the lung counting measurement. One reason is that the human body always contains radioactive substances that interfere with the measurement. Natural and man-made radionuclides enter our bodies through the food we eat and the air we breathe and are, therefore, constantly replenished. Due to this, a background due to Compton scattering is observed in the low-energy region where a scattered photon has escaped from the active volume of the detector or interacted and deposited its energy elsewhere before being recorded by the detector system. The background is always generated even if the natural background radiation outside the measured object is suppressed with an anti-Compton shield. In addition, gamma rays with energies below 100 keV are greatly attenuated by the chest wall (ICRU, 2003; Jutila et al., 2023). To overcome these issues, a long acquisition time is needed.

In naturally occurring potassium, 0.0117% is ^{40}K (Rosman and Taylor, 1998). An adult with a body mass of 70 kg has about 140 g (ICRP, 1975) of potassium in their body, meaning that on average the activity of the human body from ^{40}K is around 4300 Bq. Traces of nuclear accidents, weapon tests, and the resulting nuclear fallout from these events can also be seen in the human body. The fission product ^{137}Cs passes into the body from the soil through food and water, but the cesium concentration today in the average human body is extremely low or there is none at all, depending on the geographical area, and it is only a fraction of the average ^{40}K concentration (Mattila and Inkinen, 2023). To put this into perspective, the annual dose accumulated from artificial and natural internal sources is again only a small part of the total annual dose, which is mainly caused by radon in the air (UNSCEAR, 2010).

* Corresponding author. Accelerator Laboratory, Department of Physics, University of Jyväskylä, FI-40014 Jyväskylä, Finland.
E-mail address: henri.m.jutila@jyu.fi (H. Jutila).

https://doi.org/10.1016/j.apradiso.2024.111377
Received 8 December 2023; Received in revised form 19 May 2024; Accepted 25 May 2024
Available online 25 May 2024

However, gamma radiation from the naturally occurring ^{40}K ($E_\gamma = 1461$ keV) and man-made ^{137}Cs ($E_\gamma = 662$ keV) are the main sources of background events in lung counting measurements if the natural background radiation is suppressed, as shown in Fig. 1.

The activity concentrations due to internal contamination in the human body of various radionuclides can be low compared to the natural background radiation and therefore, lung counting measurements and long-term monitoring are usually performed in a low background chamber enclosed by a combination of steel, lead, and copper to minimize the natural background radiation and to suppress X-ray emission from lead during the measurements. In this way, the background events in the gamma-ray spectrum generated by the radionuclides in the human body can become a major factor in the measurement.

In this work, the aim was to reduce background below 100 keV using a laterally segmented HPGe detector with a thin front segment. In this way, the direct detection of extremely dangerous radionuclides that emit low-energy gamma rays, such as ^{241}Am (ATSDR, 2004) or ^{239}Pu (ATSDR, 2010), can be improved by reducing the Minimum Detectable Activity (MDA). The concept relies on the premise that the high-energy gamma rays emitted from the decays of ^{137}Cs, ^{40}K inside the ICRP adult reference computational phantom, and other radionuclides in the environment are more likely to pass through the thin front segment of the HPGe detector without interacting and scattering events are more uniformly distributed in the thicker rear segment. Operating the HPGe detector in combination with an active shield in anti-coincidence mode (Beausang et al., 1992; Długosz-Lisiecka, 2017) can further reduce the level of background. In this method, any scattered and/or escaped photons can be detected in coincidence in the rear segment and/or in the active shield and vetoed (removed) from the data. By suppressing the background, the MDA of the corresponding radionuclide is in turn reduced, lowering the limit of detection sensitivity.

2. Methods

In this section, the relevant aspects of gamma-ray attenuation and determination of MDA values will be briefly described, different detector configurations presented, and the overall working principles of the Geant4 simulations explained.

2.1. The attenuation law for gamma rays

A beam of gamma rays is attenuated when traversing through matter. Gamma rays interact with matter mainly via photoelectric absorption, Compton scattering, and pair production in the nuclear and atomic electron field. Each can be described as a probability of interaction per unit path length traversed in matter (τ, σ, κ). The sum of these probabilities is called the linear attenuation coefficient, μ, which describes the probability that a gamma ray is removed from the beam

$$\mu = \tau\,(\text{photoelectric}) + \sigma(\text{Compton}) + \kappa(\text{pair}). \tag{1}$$

The triplet production, which is a special case of pair production occurring in the atomic electron field is included in the last term. In terms of the more widely used mass attenuation coefficient, μ/ρ, the attenuation law for gamma rays is given by

$$\frac{I}{I_0} = e^{-(\mu/\rho)\rho t}, \tag{2}$$

where I is the number of gamma rays transmitted through the absorber material and I_0 is the number of gamma rays transmitted without the absorber. The product, ρt, is the mass thickness of the absorber material obtained by multiplying the thickness t by the density ρ of the absorber material.

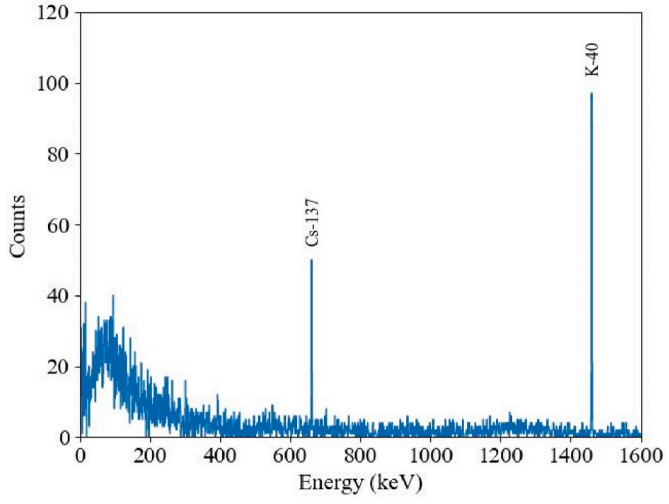

Fig. 1. A 1-h background subtracted lung counting spectrum measured at the Radiation and Nuclear Safety Authority (STUK) from a human body in a low background chamber showcasing the two radionuclides of which ^{40}K is always present in the human body.

2.2. Minimum detectable activity

Due to the inherent stochastic nature of radioactive decay, it is impossible to say when a nucleus will decay, but it is possible to predict the probability of nuclear decay per unit time. Due to the randomness, the number of decay events recorded will vary between measurements, and it is possible to make two mistakes: declare that real activity is present when it is not (false-positive) or declare that real activity is not present when it is (false-negative). To mitigate this problem, it is useful to determine the critical level L_C and the detection limit L_D. The critical level determines if a measurement is reported positive (real activity is present) or negative (real activity is not present) at a certain confidence level. The detection limit is the minimum activity present that can be detected at a certain confidence level. Using $L_C = 2.33\sigma_B$ and $L_D = L_C + 1.64\sigma_D$, where σ_B and σ_D are the standard deviations of the background and source measurements respectively, as described in the Currie definition of MDA (Currie, 1968), will lead to

$$L_D = 4.65\sqrt{N_B} + 2.71. \tag{3}$$

In the above equation, L_D is the minimum number of net counts needed to ensure 5% false-negative rate when real activity is present and when the measurement system is operated with the critical level L_C that, in turn, ensures that the false-positive rate is no more than 5%. N_B is the number of background events in the Region of Interest (ROI), for example, the width of a gamma-ray photopeak. The equation above can be transformed into the minimum detectable activity [Bq]

$$\text{MDA} = \frac{L_D}{\varepsilon_P I t}, \tag{4}$$

where $\varepsilon_P = N_P^i / N_P^{max}$ is the relative photopeak efficiency normalized by the simulation which has the highest number of photopeak events. I is the intensity or the fractional yield of the radiation per disintegration and t is the measurement time. The intensity and the measurement time are constant for all simulations thus, only L_D and ε_P are used to calculate the MDA because the relative performance of the detector configurations is of main interest and not the absolute value of the MDA which should be calculated using absolute efficiency.

2.3. Detector configurations

Various HPGe detector configurations were tested in Geant4. Each of the eight detector models adds a layer of complexity to the previous one. All detector models as visualized in Geant4 are shown in Fig. 2. The base

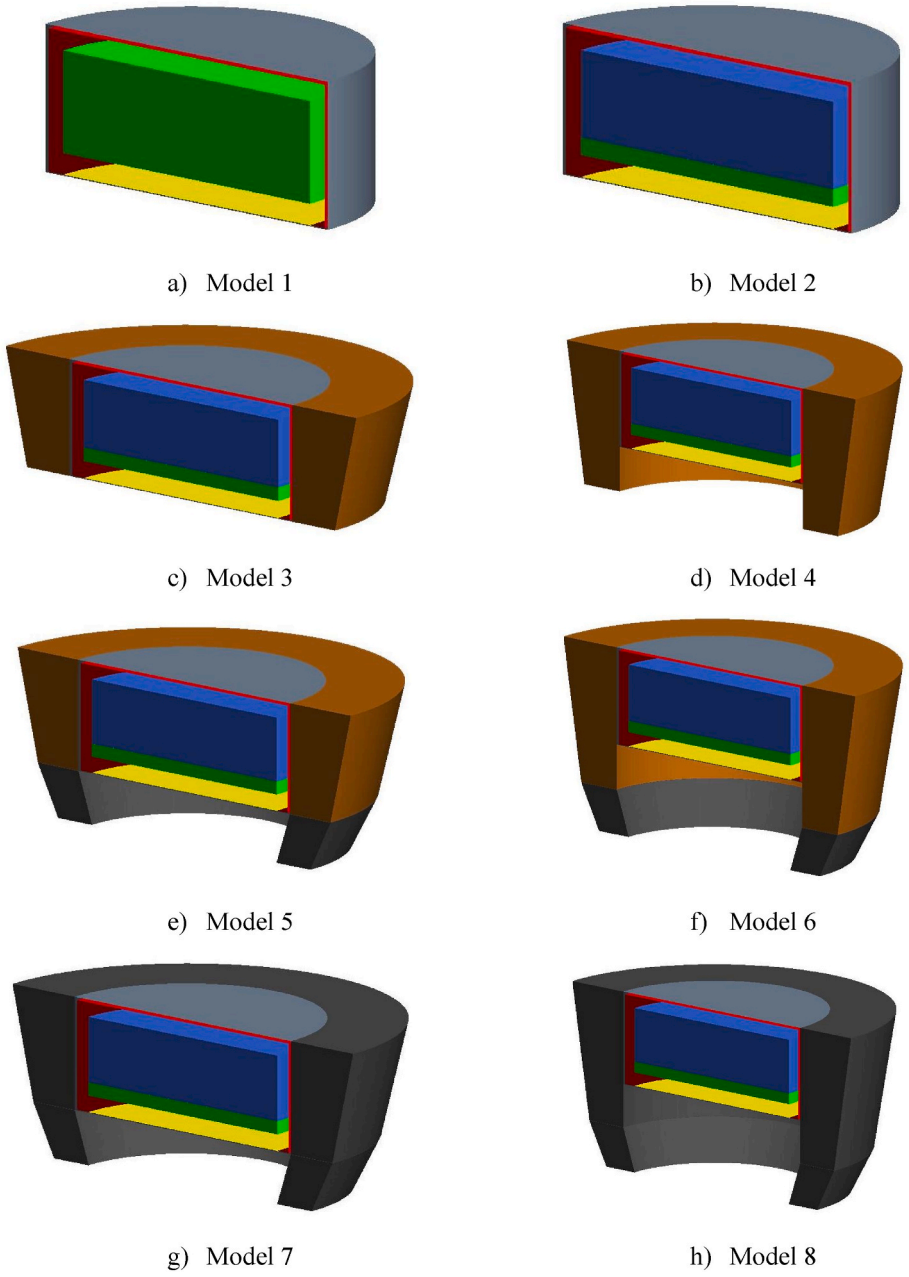

Fig. 2. Detector models used in the lung counting simulations with various active, BGO, (brown) and passive, lead, (dark grey) shield combinations together with the segmented HPGe consisting of a thin front segment (green) and thicker rear segment (blue) in vacuum (red) and enclosed by aluminium capsule (light grey). All models were also equipped with a thin beryllium window (yellow).

model (model 1) is a simple planar detector with a single germanium crystal (green) with a thickness of 30.0 mm and a radius of 45.5 mm. The crystal was enclosed by a 1.1 mm thick aluminium capsule (light grey) and a 5.5 mm vacuum space (red) between the crystal and the aluminium. All models are also equipped with 0.3 mm thick beryllium window (yellow). Model 2 introduces segmentation to the germanium crystal, which is used in all the following models. The base model crystal is divided into two segments: a 5 mm front (green) and a 25 mm rear (blue) segment. In model 3, an active annular tapered bismuth germanate (BGO) scintillator shield (brown) is attached to the aluminium capsule with a 20 mm and 30 mm outer radius. The BGO shield is elongated with a 20 mm extension outward from the beryllium window in model 4. In model 5, a 20 mm thick tapered lead collimator (dark grey) is attached to the annular BGO shield with a 62 mm and 72 mm outer radius. Model 6 is the same as model 5 but with the lead collimator attached to the extended part of the BGO shield. Finally, models 7 and 8 are the same as models 5 and 6 except that the active shield is replaced with a passive lead shield.

2.4. Geant4 simulations

An application specific Geant4 (version 10.5) simulation package for lung and whole-body counting was recently developed (Jutila et al., 2023). In this work, the package was used to investigate the performance of eight detector configurations in terms of background suppression in lung counting. The package utilizes ICRP adult reference computational phantoms and a Livermore physics library (Allison et al., 2016). A detailed description of the voxel phantoms has been given in (ICRP, 2009) but in this work, only part of the male phantom (27 slices) was used that contains the lungs to cut down the computational time.

Use of a truncated phantom is justified by the small frontal area of the detector, which makes it unlikely that scattered photons from other parts of the phantom would hit the detector and create additional background events.

Geant4 (Agostinelli et al., 2003) is a toolkit to simulate interactions of particles in matter using Monte Carlo methods. The simulations consist of tracks of particles that can be divided into steps that are defined as the distance between two interaction points (Guatelli et al., 2011). It is possible to retrieve the energy of the particle, the type of interaction that occurred, and the energy loss during each step. From the energy deposition of each step, it is possible to construct, e.g., a gamma-ray spectrum.

In simulations where the computational phantom was used, radionuclides ^{137}Cs and ^{40}K were uniformly distributed in the computational phantom, as they are found in all major soft tissues. In total, 10^7 gamma rays with energies of 662 keV and 1461 keV were emitted inside the computational phantom with arbitrary position and direction. Americium activity was also simulated in the lungs. Overall, 10^6 gamma rays with an energy of 59.5 keV, which is used to identify ^{241}Am, were emitted from the lung voxels of the computational phantom. In this case, a random emission position was selected in the computational phantom and if the material at the selected coordinates was found to be lung, the emission was processed. Otherwise, a new position was selected until the material was confirmed to be lung. Therefore, the activity was uniformly distributed in the computational lungs.

The same set of gamma rays (662 keV and 1461 keV) were emitted from inside the computational phantom such that there was no loss of intensity inside the phantom. This was achieved by replacing all phantom materials with vacuum and detecting gamma rays with detector model 1.

A set of radionuclides were also simulated, shown in Table 1 without the computational phantom to mimic the natural background radiation. The activities were determined from experimental data measured in the low background chamber at STUK. Altogether, 10^6 photons were emitted across a wide energy range from a few keV up to 3 MeV. Photons were emitted within a sphere with a radius of 200 mm enclosing the detector model. Again, the emission position and direction were randomly selected within the sphere outside the detector volume.

In all four cases, the gamma rays and photons are emitted one at a time and the steps of the tracks are stored. The steps contain information about the material volume where the interaction occurred. If the gamma ray interacted only inside the thin front segment of the HPGe detector, it was marked as a good event. If the gamma ray also interacted in the rear segment and/or in the active BGO shield, it was flagged and vetoed in the subsequent data-analysis step. Some of the possible paths and interactions of the emitted gamma rays are illustrated in Fig. 3.

Table 1
Radionuclides and their corresponding activities used to simulate the natural background radiation based on experimental data measured in the low background chamber in the whole-body counting laboratory at STUK.

Nuclide	Activity [Bq]
^{40}K	3839
^{56}Co	33
^{57}Co	8
^{60}Co	17
^{133}Xe	70
^{137}Cs	66
^{155}Eu	98
^{208}Tl	296
^{210}Pb	733
^{212}Bi	428
^{214}Bi	470
^{214}Pb	422
^{224}Ra	1109
^{228}Ac	308
^{234}Th	9128
^{234m}Pa	12899
^{235}U	671

The width of the 59.5 keV gamma-ray photopeak was selected as the ROI, and the number of background events in the ROI was compared between the different detector models in the post-simulation analysis. The width of the ROI corresponded to 1.25 times the Full Width at Half Maximum (FWHM) of the 59.5 keV photopeak to ensure 99.6% peak coverage. An energy resolution function was also implemented in the simulations determined from experimental data (Jutila et al., 2023).

All detector configurations used in the simulations were ideal, i.e., all interactions inside the active volumes were recorded and no losses due to dead time, dead layers, or improper charge collection were taken into account. The statistical uncertainties of the simulations were minimized by using a large photon sample size, a small simulation tracking cut, and a high spatial resolution of the phantom.

3. Results

3.1. The attenuation of photons in germanium

The attenuation of low-energy photons in germanium for energies 20 keV–150 keV was calculated with Eq. (2) using mass attenuation coefficients from the National Institute of Standards and Technology (NIST) (Hubbell & Seltzer). The thickness of the germanium crystal as a function of the photon attenuation is shown in Fig. 4. Guided by the attenuation values, the thin front segment was chosen to be 5 mm thick in the lateral direction in order to guarantee maximum efficiency for detection of gamma rays up to an energy of around 80 keV in the front segment. The 5 mm front segment was then used in detector models 2–8.

3.2. Background events generated by internal sources

Natural ^{40}K and man-made ^{137}Cs activities were simulated inside the ICRP adult reference computational phantom. Due to the activities already present in the human body, a lung counting spectrum always contains a background component that cannot be removed. This was demonstrated by replacing the phantom materials with vacuum so that the loss of gamma-ray intensity due to the various tissues found in the phantom was minimized. In addition, ^{241}Am contamination inside the

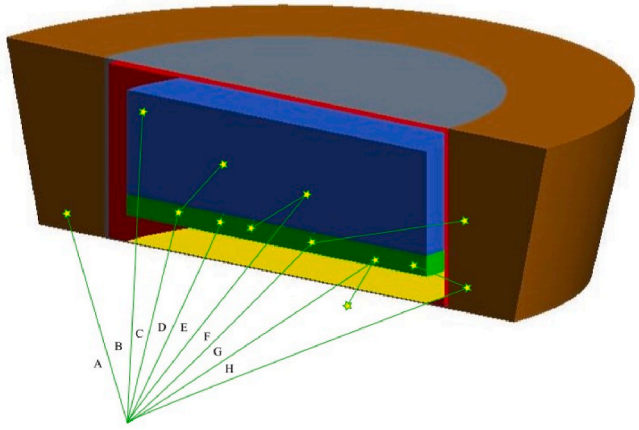

Fig. 3. Illustration of some of the possible paths and interactions of emitted primary gamma rays (A–H) that can occur in the Geant4 simulation environment. From the interaction points (stars), it is possible to retrieve the deposited energy and construct a gamma-ray spectrum. Only event D is considered as a good event and all others will be vetoed except event G which is considered as background event. However, if the photon interacted in the computational phantom before being detected by the detector, even event D could be considered as a background event.

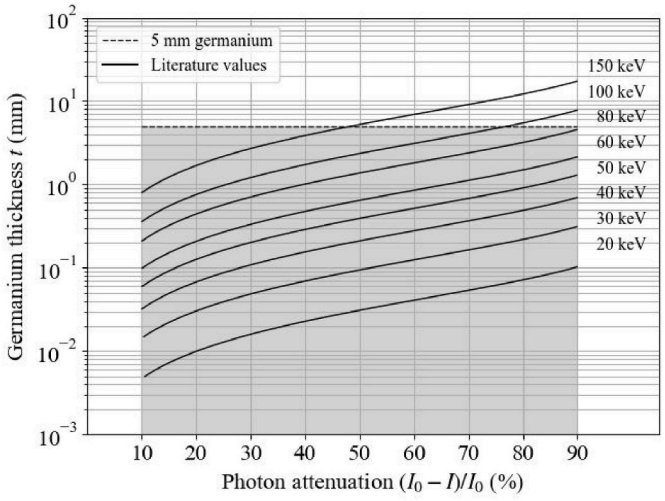

Fig. 4. Attenuation of low-energy photons traversing through germanium (Hubbell & Seltzer). Photon energies below 100 keV are greatly attenuated by 5 mm of germanium crystal, visualized with the grey background color.

lungs was simulated and the total number of background events in the ROI was detected. It was observed that the background level in the ROI was 2.5 times higher with the normal computational phantom compared to the vacuum phantom shown in Fig. 5a when detected with model 1.

The internal activities were also detected with detector models 1 and 2 using the normal computational phantom. Events generated through Compton scattering which result in energy deposition in both the thin front segment and the thicker rear segment of model 2 were vetoed. The background events in the ROI detected with the two models are shown in Fig. 5b (note the logarithmic y-scale). The number of background events was reduced by 45% when the two models were compared. Using the relative photopeak efficiency of the 59.5 keV gamma rays, ε_P, the number of background events under the photopeak, N_B, and equations (3) and (4), it was calculated that the deduced MDA was reduced by 21%.

Various BGO and lead shield configurations were modeled together with the segmented HPGe detector (models 3–8). It was investigated if the shielding of the detector had any major effect on the background events generated in the low-energy region by radionuclides inside the computational phantom. It was observed that a further reduction of 55% of the original background level was obtained, corresponding to a 30% reduction in the MDA when detector models 1 and 3 were compared. Simulation results using all models are shown in Table 2.

It should be noted that the cesium and potassium activities in the simulations correspond to realistic activity levels found in the human body (as shown in Fig. 1) but also to many hours of acquisition time (5–10 h) and do not, in that sense, represent real lung counting measurements. This approach was taken in order to accumulate sufficient statistics below the 59.5 keV photopeak to allow a quantitative comparison between different detector configurations.

3.3. Background events generated by external sources

The natural background radiation was suppressed with different BGO and lead shield configurations around the segmented HPGe detector. Sets of gamma rays related to the decays of radionuclides in Table 1 were emitted around each of the detector models in the Geant4 environment to roughly mimic the natural background radiation. The simulated spectra measured with detector models 1 and 3 are shown in Fig. 5c, where background events in the ROI are highlighted. The background under the photopeak used to identify ^{241}Am in lung counting was reduced by 91% which translates to a 66% reduction in the MDA. More detailed results for each detector model are shown in Table 2.

4. Discussion and conclusion

A segmented HPGe detector with a thin front segment and a thicker rear segment was modeled in a Geant4 environment with different active and passive shield configurations, shown in Fig. 2. The aim was to improve the detection of 59.5 keV gamma rays and in turn lower the minimum detectable activity of inhaled ^{241}Am inside the lungs. A Geant4 simulation package for lung counting utilizing the ICRP adult reference computational phantom was used to benchmark the segmented HPGe detector performance with different shield configurations.

Based on the attenuation of low-energy photons in germanium, a 5 mm front segment was selected for the detection of gamma rays with energies below 100 keV. The attenuation of 20 keV–150 keV photons is shown in Fig. 4. Whilst in principle the front segment could perhaps be slightly thinner and maintain efficiency up to 60 keV, the choice is also a minor compromise based on discussions with a potential manufacturer of what is technologically possible for proper charge collection and still maintain a good detection efficiency for gamma and X-rays below 100 keV. The selected thickness also enables the detection of slightly higher energy gamma and X-rays originating from elements such as uranium and radium that are naturally occurring but also from gallium, technetium, iodine, xenon, thallium, and lutetium that are widely used in the field of nuclear medicine. The diameter was also modeled based on existing detector geometries.

Ideal detectors were chosen for this application so that all interactions in the detector materials were stored, and no dead layer was implemented, since the main goal was not to replicate experimental data or use the simulations for quantitative analysis of real-world MDA. Instead, the aim was to estimate how much internal and external background in lung counting can be reduced with segmentation and with use of anti-Compton suppression shield and to make relative comparison of the different configurations. In addition, the dead layer can be assumed to be only a few μm thick in a Broad Energy Germanium (BEGe) detector (Woodroof et al., 2022). Thus, there would be only a minimal effect on the detection of 59.5 keV gamma rays. The effect due to the dead layer would be very similar in all cases and would be mostly cancelled out when looking at relative differences between the detector models and not the absolute values.

A uniform distribution of ^{137}Cs and ^{40}K activity was deposited inside the computational phantom, and the reduction in background under the 59.5 keV photopeak was measured. It is clear from Fig. 5a that in lung counting measurements, there exists a background component that cannot be removed or suppressed, which is due to the gamma rays interacting inside the computational phantom before they are detected by the measurement system even if the natural background radiation would be completely suppressed. The effect of such events is also 1.5 times larger than the effect due to the scattering events inside the active volume of the detector that eventually leads to the gamma rays escaping the detector. This finding is important, as it means that there are some background contributions that cannot be removed in the measurements.

The simulated spectra centered on the 59.5 keV (^{241}Am) photopeak for models 1 and 2 are shown in Fig. 5b, and more detailed results are shown in Table 2 for each detector model. The results show that the background events in the thin front segment after vetoing of scattered events can be reduced by 45% which corresponds to a 21% reduction in MDA. On the other hand, some photopeak events are lost due to the segmentation since the angle of acceptance is smaller for gamma rays detected from the side of the detector, which can be seen in the decrease of the relative photopeak efficiency of 59.5 keV gamma rays. The reduction of background events in the region of interest results in improved MDA values for the segmented HPGe. Background events in the ROI can be further reduced by 55% compared to the original background level obtained using detector model 1 corresponding to a 30%

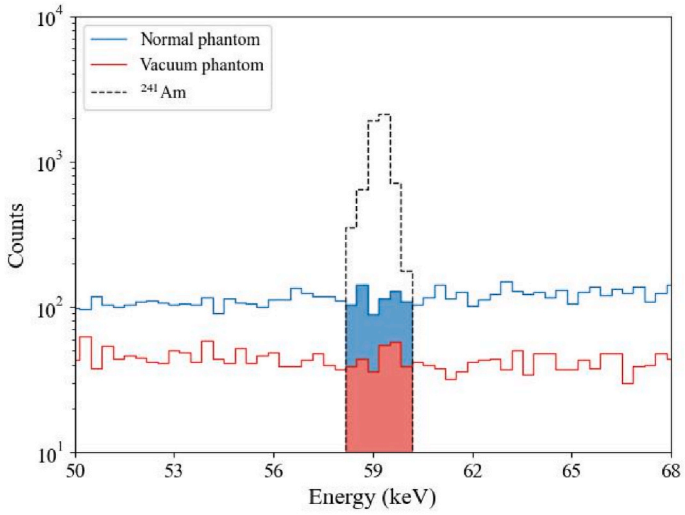

a)

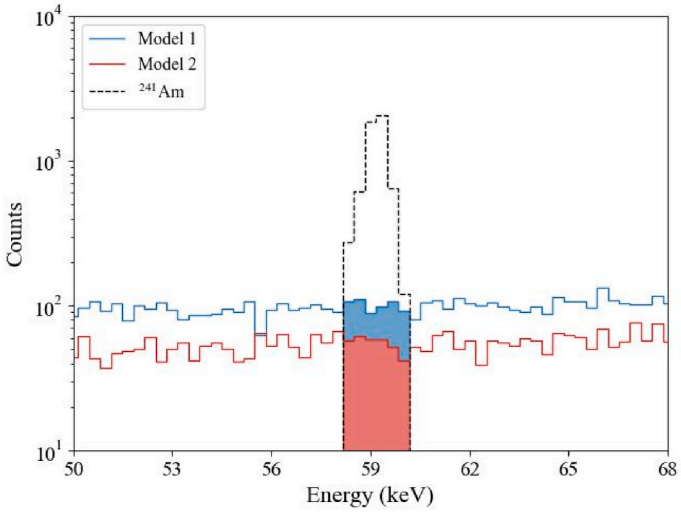

b)

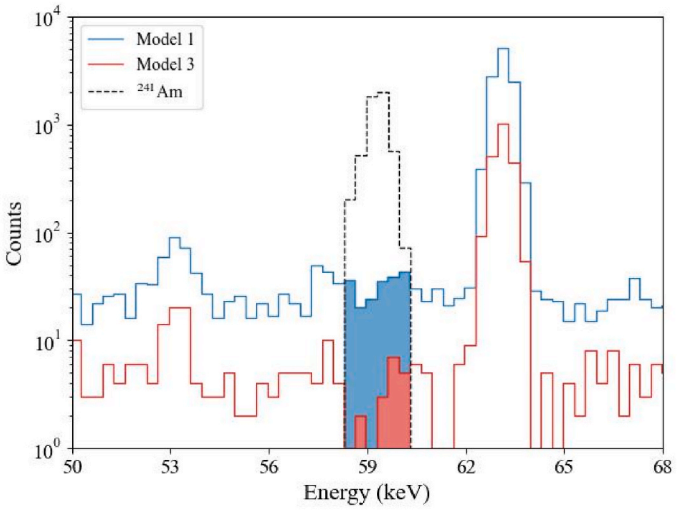

c)

Fig. 5. Background events highlighted under the 59.5 keV (^{241}Am) photopeak generated in the simulated lung counting spectrum a) by internal sources (^{137}Cs and ^{40}K) detected with model 1 using the normal computational phantom and a modified phantom where tissues were replaced with vacuum. b) by internal sources detected with models 1 and 2 and c) by external sources detected with models 1 and 3.

Table 2
The calculated MDA, relative photopeak efficiency ε_P, and the detection limit L_D for each detector model based on background counts N_B under the 59.5 keV photopeak generated by ^{137}Cs and ^{40}K inside the ICRP computational phantom (internal) and the gamma rays from the environment (external).

Det.	N_B [counts]		L_D [counts]		ε_P [%]	MDA [Bq]		ΔMDA [%]	
Mod.	Int.	Ext.	Int.	Ext.	^{241}Am	Int.	Ext.	Int.	Ext.
1	604(25)	197(15)	117(37)	68(22)	100(3)	117(37)	68(22)	0	0
2	332(19)	34(6)	87(28)	30(10)	94(2)	93(30)	32(11)	−21	−53
3	274(17)	18(5)	80(26)	22(8)	97(2)	82(26)	23(8)	−30	−66
4	285(17)	21(5)	81(26)	24(9)	95(2)	85(27)	25(9)	−27	−63
5	297(18)	20(5)	83(27)	24(8)	93(2)	89(29)	25(9)	−24	−63
6	261(17)	22(5)	78(25)	25(9)	94(2)	83(27)	26(9)	−29	−61
7	341(19)	35(6)	89(28)	30(11)	93(2)	95(30)	33(11)	−18	−52
8	295(18)	24(5)	83(26)	25(9)	93(2)	88(28)	27(10)	−24	−60

reduction in the MDA by using an active shield (model 3) around the germanium crystal. However, adding additional components to the shield did not yield improved results. Model 6 has the lowest background out of the eight models but because of the relatively poor detection efficiency, the MDA is essentially the same for the two detector models.

The natural background radiation was mimicked by simulating gamma and X-rays emitted from decays of radionuclides (see Table 1) in the uranium, thorium and other series found in nature, based on an experimentally measured spectrum. The simulation was performed for each of the detector configurations without the computational phantom. Again, the performance was determined by investigating the reduction of the background level in the ROI. The simulated spectra measured using detector models 1 and 3 are shown in Fig. 5c. A significant reduction of background events in the ROI can be seen when comparing models 1 and 2 but overall model 3 has the lowest MDA which is reduced by 66% when compared to model 1. In turn, this means that the background events in the thin segment were reduced by 91%. However, the results for all the active shield models are all equivalent within the margin of error. Surprisingly, the passive shield models give similar or worse results to those with no shield at all, which is due to the X-ray emissions of lead at around 70 keV.

In reality, the ^{137}Cs and ^{40}K simulations correspond to many hours of acquisition time of a typical experimental lung counting measurement, but internal background can have a major effect in the final spectrum when measuring in a low background chamber where the natural background level can be 1% of the level outside the chamber. However, these results show that it is possible to reduce the detection limit or the measurement time using the segmented HPGe detector in low background chamber measurements. In addition, combining the detector application with an active shield would be particularly useful in field measurements in which suppression of the background radiation is essential. In the future, the results of the simulations will be replicated and verified via measurements with a segmented prototype detector and active and passive shielding.

CRediT authorship contribution statement

Henri Jutila: Writing – review & editing, Writing – original draft, Visualization, Software, Investigation, Formal analysis. **Paul Greenlees:** Writing – review & editing, Supervision, Methodology, Conceptualization. **Tiina Torvela:** Writing – review & editing. **Maarit Muikku:** Writing – review & editing, Methodology, Conceptualization.

Declaration of competing interest

The authors declare that they have no known competing financial interests or personal relationships that could have appeared to influence the work reported in this paper.

Data availability

Data will be made available on request.

References

Agostinelli, S., Allison, J., Amako, K., Apostolakis, J., Araujo, H., Arce, P., Asai, M., Axen, D., Banerjee, S., Barrand, G., Behner, F., Bellagamba, L., Boudreau, J., Broglia, L., Brunengo, A., Burkhardt, H., Chauvie, S., Chuma, J., Chytracek, R., Cooperman, G., Cosmo, G., Degtyarenko, P., Dell'Acqua, A., Depaola, G., Dietrich, D., Enami, R., Feliciello, A., Ferguson, C., Fesefeldt, H., Folger, G., Foppiano, F., Forti, A., Garelli, S., Giani, S., Giannitrapani, R., Gibin, D., Gómez Cadenas, J.J., González, I., Gracia Abril, G., Greeniaus, G., Greiner, W., Grichine, V., Grossheim, A., Guatelli, S., Gumplinger, P., Hamatsu, R., Hashimoto, K., Hasui, H., Heikkinen, A., Howard, A., Ivanchenko, V., Johnson, A., Jones, F.W., Kallenbach, J., Kanaya, N., Kawabata, M., Kawabata, Y., Kawaguti, M., Kelner, S., Kent, P., Kimura, A., Kodama, T., Kokoulin, R., Kossov, M., Kurashige, H., Lamanna, E., Lampén, T., Lara, V., Lefebure, V., Lei, F., Liendl, M., Lockman, W., Longo, F., Magni, S., Maire, M., Medernach, E., Minamimoto, K., Mora de Freitas, P., Morita, Y., Murakami, K., Nagamatu, M., Nartallo, R., Nieminen, P., Nishimura, T., Ohtsubo, K., Okamura, M., O'Neale, S., Oohata, Y., Paech, K., Perl, J., Pfeiffer, A., Pia, M.G., Ranjard, F., Rybin, A., Sadilov, S., Di Salvo, E., Santin, G., Sasaki, T., Savvas, N., Sawada, Y., Scherer, S., Sei, S., Sirotenko, V., Smith, D., Starkov, N., Stoecker, H., Sulkimo, J., Takahata, M., Tanaka, S., Tcherniaev, E., Safai Tehrani, E., Tropeano, M., Truscott, P., Uno, H., Urban, L., Urban, P., Verderi, M., Walkden, A., Wander, W., Weber, H., Wellisch, J.P., Wenaus, T., Williams, D.C., Wright, D., Yamada, T., Yoshida, H., Zschiesche, D., 2003. Geant4—a simulation toolkit. Nucl. Instrum. Methods Phys. Res. 506, 250–303. https://doi.org/10.1016/S0168-9002(03)01368-8.

Allison, J., Amako, K., Apostolakis, J., Arce, P., Asai, M., Aso, T., Bagli, E., Bagulya, A., Banerjee, S., Barrand, G., Beck, B.R., Bogdanov, A.G., Brandt, D., Brown, J.M.C., Burkhardt, H., Canal, Ph, Cano-Ott, D., Chauvie, S., Cho, K., Cirrone, G.A.P., Cooperman, G., Cortés-Giraldo, M.A., Cosmo, G., Cuttone, G., Depaola, G., Desorgher, L., Dong, X., Dotti, A., Elvira, V.D., Folger, G., Francis, Z., Galoyan, A., Garnier, L., Gayer, M., Genser, K.L., Grichine, V.M., Guatelli, S., Guèye, P., Gumplinger, P., Howard, A.S., Hřivnáčová, I., Hwang, S., Incerti, S., Ivanchenko, A., Ivanchenko, V.N., Jones, F.W., Jun, S.Y., Kaitaniemi, P., Karakatsanis, N., Karamitros, M., Kelsey, M., Kimura, A., Koi, T., Kurashige, H., Lechner, A., Lee, S.B., Longo, F., Maire, M., Mancusi, D., Mantero, A., Mendoza, E., Morgan, B., Murakami, K., Nikitina, T., Pandola, L., Paprocki, P., Perl, J., Petrović, I., Pia, M.G., Pokorski, W., Quesada, J.M., Raine, M., Reis, M.A., Ribon, A., Ristić Fira, A., Romano, F., Russo, G., Santin, G., Sasaki, T., Sawkey, D., Shin, J.I., Strakovsky, I.I., Taborda, A., Tanaka, S., Tomé, B., Toshito, T., Tran, H.N., Truscott, P.R., Urban, L., Uzhinsky, V., Verbeke, J.M., Verderi, M., Wendt, B.L., Wenzel, H., Wright, D.H., Wright, D.M., Yamashita, T., Yarba, J., Yoshida, H., 2016. Recent developments in Geant4. Nucl. Instrum. Methods Phys. Res. 835, 186–225. https://doi.org/10.1016/j.nima.2016.06.125.

ATSDR, 2010. Toxicological Profile for Plutonium. U.S. Department of Health and Human Services, Public Health Service, Atlanta, GA.

ATSDR, 2004. Toxicological Profile for Americium. U.S. Department of Health and Human Services, Public Health Service, Atlanta, GA.

Beausang, C.W., Forbes, S.A., Fallon, P., Nolan, P.J., Twin, P.J., Mo, J.N., Lisle, J.C., Bentley, M.A., Simpson, J., Beck, F.A., Curien, D., deFrance, G., Duchêne, G., Popescu, D., 1992. Measurements on prototype Ge and BGO detectors for the Eurogam array. Nucl. Instrum. Methods Phys. Res. 313, 37–49. https://doi.org/10.1016/0168-9002(92)90084-H.

Currie, L.A., 1968. Limits for qualitative detection and quantitative determination. Application to radiochemistry. Anal. Chem. 40, 586–593. https://doi.org/10.1021/ac60259a007.

Długosz-Lisiecka, M., 2017. Application of modern anticoincidence (AC) system in HPGe γ-spectrometry for the detection limit lowering of the radionuclides in air filters. J. Environ. Radioact. 169–170, 104–108. https://doi.org/10.1016/j.jenvrad.2017.01.008.

Guatelli, S., Cutajar, D., Oborn, B., Rosenfeld, A.B., Rosenfeld, A., Kron, T., d'Errico, F., Moscovitch, M., 2011. Introduction to the Geant4 simulation toolkit. AIP Conf. Proc. 1345, 303–322. https://doi.org/10.1063/1.3576174.

ICRP, 2009. Adult Reference Computational Phantoms, 110. ICRP Publication. Ann ICRP 39.

Hubbell, J.H., Seltzer, S.M., n.d. Tables of X-ray mass attenuation coefficients and mass energy-absorption coefficients (version 1.4). National Institute of Standards and Technology, Gaithersburg, MD. http://physics.nist.gov/xaamdi (Accessed 11 May 2024).

ICRP, 1975. Report of the Task Group on Reference Man. ICRP Publication 23. Pergamon Press, Oxford.

ICRU, 2003. Direct determination of the body content of radionuclides. ICRU Report 69. J. ICRU 3.

Jutila, H., Greenlees, P., Torvela, T., Muikku, M., 2023. Technical note: simulation of lung counting applications using Geant4. Phys. Med. 108 https://doi.org/10.1016/j.ejmp.2023.102573.

Mattila, A., Inkinen, S. (Eds.), 2023. Environmental Radiation Monitoring in Finland. Annual Report 2022. STUK-B 304, Helsinki.

Rosman, K.J.R., Taylor, P.D.P., 1998. Isotopic compositions of the elements 1997 (Technical Report). Pure Appl. Chem. 70, 217–235. https://doi.org/10.1351/pac199870010217.

UNSCEAR, 2010. Sources and Effects of Ionizing Radiation 2008 Report, Volume I. https://doi.org/10.18356/cb7b6e26-en. UN, New York.

Woodroof, T.F., Boston, A.J., Judson, D.S., 2022. Monte Carlo simulation of a BEGe 6530 detector in GAMOS. Nucl. Instrum. Methods Phys. Res. 1034, 166726 https://doi.org/10.1016/j.nima.2022.166726.